Ablative Rayleigh-Taylor Instability at Short Wavelengths Observed with Moiré Interferometry

T. Sakaiya, H. Azechi, M. Matsuoka, N. Izumi, M. Nakai, K. Shigemori, H. Shiraga, A. Sunahara,
H. Takabe, and T. Yamanaka
Institute of Laser Engineering, Osaka University, 2-6 Yamada-Oka, Suita, Osaka 565-0871, Japan

(Received 16 April 2001; published 25 March 2002)

One of the most important quantities to be measured for better understanding of the ablative Rayleigh-Taylor (RT) instability is the growth rate in the short wavelength region at which the RT instability is significantly reduced. The short wavelength (4.7–12 μm) RT growth rates for direct-drive targets were measured for the first time by utilizing the innovated moiré interferometry [M. Matsuoka *et al.*, Rev. Sci. Instrum. **70**, 637 (1999)]. These growth rates were reasonably well reproduced by the simulation that solves the Fokker-Planck equation for nonlocal heat transport.

DOI: 10.1103/PhysRevLett.88.145003 PACS numbers: 52.35.Py, 52.50.Jm, 52.70.La

The Rayleigh-Taylor (RT) instability [1] is a well-known classical fluid phenomenon that takes place when a heavy fluid is accelerated by a light fluid. However, the RT instability in inertial confinement fusion (ICF) targets and in some astrophysical objects, such as type Ia supernovae [2] and interstellar clouds irradiated by O stars [3], have an essential difference from the classical problem. In these nonclassical situations, there exist intense energy sources in the light fluid: laser absorption in ICF targets, C and O burning in Type Ia supernovae, and UV absorption in interstellar clouds. The energy is absorbed and transported to the interface between the heavy and light fluids, resulting in the ablation of the heavy fluid. Since the ablation removes the RT perturbation away from the unstable surface, the RT growth is reduced from its classical growth. The growth rate γ of the RT instability that includes the ablation effect (so called the ablative RT) has been suggested by Bodner [4], and is approximated by the modified Takabe formula [5]:

$$\gamma = \sqrt{kg/(1 + kL)} - \beta k v_a, \tag{1}$$

where k is the wave number of the perturbation, g is the gravity, L is the density scale length at the ablation surface, v_a is the fluid velocity across the unstable surface, and the factor β depends on the ablation structure which is determined by energy transport processes. Takabe *et al.* [5] have determined the value of β for hydrogen plasmas with electron energy transport to be $\beta = 3$–4. Betti *et al.* [6] have found the analytical solution that is approximated by Eq. (1). They predict that the x-ray transport modifies the plasma density profile, resulting in $\beta = 1.7$ for plastic ICF targets.

As is expected from Eq. (1), the ablative stabilization is more pronounced for shorter wavelengths (in the present experimental condition, $\lambda \lesssim 10$ μm). This is because the RT perturbation is localized in the vicinity of the unstable surface with the spatial extent of the order of the perturbation wavelength. Therefore the ablative RT instability at short wavelengths will be a critical test of various theories [4–7]. Although there are a number of experimental studies on the ablative RT instability [8–11], few experimental studies have addressed the short wavelength RT instability because the wavelength of interest is around or even below the diagnostic spatial resolution. The shortest wavelength observed to date is 16 μm for direct drive [9] and 10 μm for indirect drive [12]. In this Letter, we will report the shortest wavelength RT instability which is measured for the first time by utilizing the newly innovated moiré interferometry [13].

The schematic view of the experimental setup is shown in Fig. 1. The target with imposed perturbation is accelerated by a drive laser and is diagnosed with the backlighting x ray emitted from a high-Z foil that is irradiated by a separate laser. The intensity distribution of the x ray transmitted through the target is imaged onto an x-ray streak camera (XSC). Areal-density perturbation is thus recorded as a contrast of the x-ray intensity distribution. This technique is referred as "face-on backlighting." The system of the moiré interferometry is just the same as that of the face-on backlighting but locating a one-dimensional grid mask, which has a period slightly different from that of the perturbation wavelength, behind the target. It is set so that the grid and the perturbation groove are parallel to each other. Because of the moiré interference between the overlapped patterns, the short wavelength perturbation of the target is converted to longer wavelength perturbations.

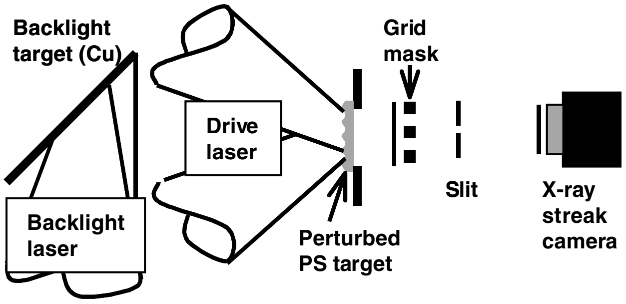

FIG. 1. The schematic view of the experimental setup for the measurement of the areal-density perturbation.

The perturbation wave number of k_1 and the grid wave number of k_2 yield the first order wave number of moiré fringe of $|k_1 - k_2|$. Areal-density perturbation with the wave number of k_1 is obtained from that of this moiré fringe. Another component $|k_1 + k_2|$ is not observed in most cases because of the limited spatial resolution of a diagnostic system. Before applying the moiré interferometry on the observation of the RT instability, we have tested the moiré technique itself. A corrugated target with carefully inspected perturbation amplitude (1.4 and 2.8 μm) was diagnosed with the same moiré technique except that the target was undriven by the laser so that the perturbation was kept unchanged. The perturbation amplitudes deduced from the moiré fringe were in excellent agreement with the actual values, ensuring the validity of the moiré technique.

The targets were made of polystyrene (PS) with a density of 1.06 g/cm^3 and a thickness of 16 μm. Sinusoidal surface perturbation was imposed on the laser irradiation side of the target by using the Fourier laser machining [14]. The target surface was coated with a 0.03-μm-thick Al to prevent early penetration of the laser light into the target. The perturbation wavelengths were 4.7, 5.7, 8.5, and 12 μm, and initial amplitudes were 0.05, 0.05, 0.1, and 0.1 μm, respectively. As for the drive laser, we used the 0.53-μm wavelength partially coherent light (PCL) [15], which was delivered from the GEKKO XII glass laser system [16], to sufficiently reduce the initial imprint of the nonuniformity in laser irradiation. The time-averaged nonuniformity of the PCL was 2%–3%. The laser intensity was 0.7×10^{14} W/cm^2 and the incident angle of the drive laser was 31.7°. The pulse shape had a nearly flat top shape with a temporal fluctuation of ±15% and had a full width at half maximum of 2.2 ns. The spot diameter was about 600 μm. The rise time and decay time of the pulse were 50 and 150 ps, respectively. We defined the time zero ($t = 0$ ns) as a time of the first half maximum. The grid mask located behind the target was made of a 2.2-μm-thick Ta with the x-ray attenuation of $\sim 10^{-4}$ for the backlighting x ray. The period of the grid was either 5 μm for the shorter wavelengths (4.7 and 5.7 μm) or 10 μm for the longer wavelengths (8.5 and 12 μm). The width of the grid was equal to that of the open space. The distance between the PS target and the grid mask was 300 μm. This distance is large enough for the flying target not to interfere with the grid even at the end of the drive laser. With this distance, the diffraction smearing (0.06 μm) of the backlighting x ray is negligibly smaller than the perturbation wavelength.

A Cu foil was used for backlighter targets. A Mg foil of 5-μm thickness was placed between the backlighter and the PS target to avoid heating of the PS target due to the soft x-ray emission from the backlighter. We also placed another 5- or 10-μm-thick Mg foil in front of the grid mask to protect the grid mask from the x-ray emission of the PS target. A transmitted x-ray image was obtained by a slit (10×50 μm^2) with magnification of 26 onto a CuI photocathode of the XSC. A Mg filter of 5-μm thickness or an Al filter of 0.8-μm thickness was located in front of the photocathode of the XSC to eliminate background emission. The temporal resolution of the XSC for the measurement was about 90 ps. The modulation transfer function (MTF) of the whole diagnostic system was measured using a backlit Frenel zone plate [13]. The nominal resolution defined as the point where MTF becomes 5% is 13 μm, and the value of MTF at the typical moiré wavelength (60 μm) is 0.74.

The target trajectory was also measured with a side-on backlighting technique where the target is backlit from its edge direction with Al x rays. Both the experiment and the simulation (explained later) show that the shock breaks out at $t = 0.4$–0.5 ns. The accelerated trajectory with average gravity of $g = (4.8 \pm 0.4) \times 10^{15}$ cm/s^2 also agrees with the simulation result. The simulation also predicts that the acceleration starts at $t = 0.5$–0.6 ns when the rarefaction wave reaches the front surface.

An example of the raw images of the face-on experiment is shown in Fig. 2(a). Although the perturbation wavelength (8.5 μm) is below the spatial resolution (13 μm), the moiré fringe (57 μm) growing with time is clearly observed. It is also seen that the wavelength of the moiré fringe increases with time. This is because the wavelength of the moiré fringe is sensitive to the wavelength difference of the two patterns. The actual change of the perturbation wavelength is only about a few percent, and therefore, its influence to the RT growth can be neglected. The raw image is line scanned at various observation times. The line scan data are fast Fourier transformed and high frequency noise is filtered out with Wiener inverse filter that include the effect of the MTF of the diagnostic system. The filtered data are then normalized by the spatial distribution of the backlighter profile, as is shown in Fig. 2(b). The noise level at the moiré wavelength is equivalent to the areal-density perturbation of 0.2 μm g/cm^3. This is about 1/3 of the minimum areal-density perturbation used for the analysis. The areal-density perturbation was then obtained from the perturbation amplitude of the normalized x-ray

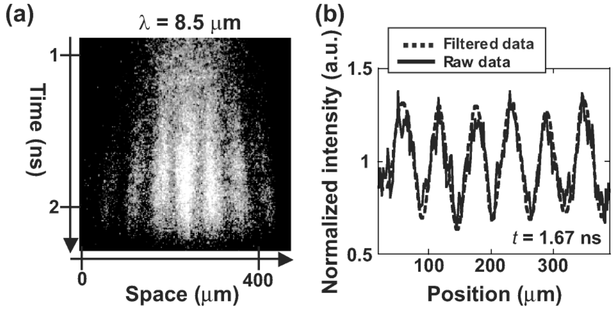

FIG. 2. (a) The streaked image of the RT experiment with moiré interferometry for $\lambda = 8.5$ μm. (b) The filtered data that are normalized by the spatial distribution of the backlighter profile and that of the raw data at $t = 1.67$ ns.

distribution divided by the mass absorption coefficient and by a first order Fourier coefficient of the rectangular function of the grid mask. Figure 3 shows the time evolution of the growth factors of the fundamental mode, where the growth factor is defined as the measured areal-density perturbation divided by the initial value.

The growth rate of the RT instability should be obtained from the exponential fit to the data of the growth factor that are in a linear growth regime. We have defined the linear regime as the period starting from the rarefaction breakout to the time at which the saturation occurs. It is observed that there is a significant growth even at the shock breakout time: Growth factors at the shock breakout are extrapolated to be 9.6 and 3.7 for the perturbation wavelength of 5.7 and 12 μm, respectively. Two mechanisms account for this early growth. One is the lateral mass flow associated with the rippled shock propagation [17]. It has been shown that if the shock propagation distance is larger than the perturbation wavelength, as in the present case, the rippled shock becomes a nearly plane shock because of the decaying oscillation of the rippled shock. This shock flattening together with the incompressibility behind the shock gives that the growth factor of the areal-density perturbation due only to the rippled shock propagation is equal to the shock compression ratio, that is, about 4. Another is the growth of the ablation front perturbation due to the Richtmyer-Meshkov (RM) like instability. In the classical RM instability [18], the perturbation grows linearly in time. On the contrary, the growth of the ablation-front perturbation is significantly reduced because of the mechanism referred as the fire-polishing effect [19] or the dynamic overpressure [20] at the ablation front. The perturbation growth factor at the shock breakout time is calculated to be 1.5 for 10-μm wavelength and 1 for 60-μm wavelength [19]. Thus, the rippled shock propagation together with RM like instability at the ablation front set up the large growth before the shock breakout.

At the later time when the perturbation amplitude of the RT instability becomes a significant fraction of the perturbation wavelength, the RT growth saturates. The saturation is often picked up as an appearance of higher harmonics of the perturbation. In the present experiment, however, the moiré interferometry observes fundamental mode only. We therefore assumed that the saturation occurs when the amplitude becomes $1/2\pi$ of the wavelength. This amplitude times the target density ($\rho = 1.6$ g/cm^3) calculated from the simulation gives the saturation level of the areal-density perturbation, which growth factor is approximately 25. This is consistent with the saturation of the growth factor observed in Fig. 3.

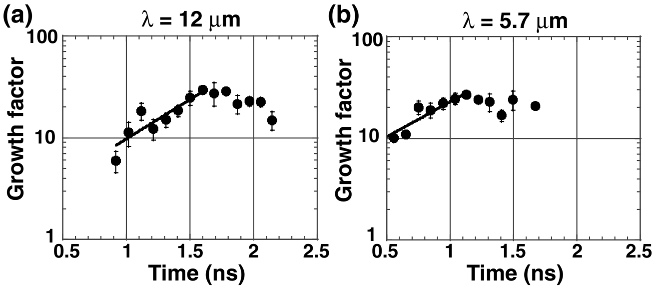

FIG. 3. The growth factor of the perturbation amplitude as a function of time for (a) $\lambda = 12$ μm and (b) $\lambda = 5.7$ μm. The lines show the exponential fitting. The gradients of these lines show the RT growth rates.

The growth rates were compiled in Fig. 4 together with the previous data [9] (closed squares). The closed circles represent the data obtained from the present experiment. The classical growth rates (dotted curve) calculated from the measured gravity are drawn as a reference. The other curves are calculated with the results of the hydrodynamic code "ILESTA-1D" [21] (with the Spitzer-Härm treatment [22] with the flux limiter of $f = 0.1$ and the Fokker-Planck treatment [23,24] for the electron heat transport). To calculate the growth rate, we solved a differential equation $d^2a(t)/dt^2 = \gamma(t)^2 a(t)$ for the perturbation amplitude $a(t)$, where the growth rate $\gamma(t)$ is given by Eq. (1) with $g(t)$, $L(t)$, and $v_a(t)$ obtained from the ILESTA-1D, and $\beta = 1.7$ is assumed. The exact value of β calculated from the Froude number and the power index for thermal conduction agrees with the approximated value of β for both the Spitzer-Härm and the Fokker-Planck treatment cases. We then calculated the areal-density perturbation by taking into account the feedthrough of the surface perturbation from the ablation front to the rear surface. The specific procedure for this is described in Ref. [9].

The experimental RT growth rates are smaller than the simulation results with the Spitzer-Härm electron transport. There are several possibilities to reduce the growth rate [9]. One of the probable candidates to reduce the growth rate is preheating due to the nonlocal heat transport [9–11]. When electron mean free path exceeds 5–10% of temperature scale length [25], high-energy electrons in a tail of a Maxwell distribution may penetrate into and preheat the target, thereby reducing the target density and

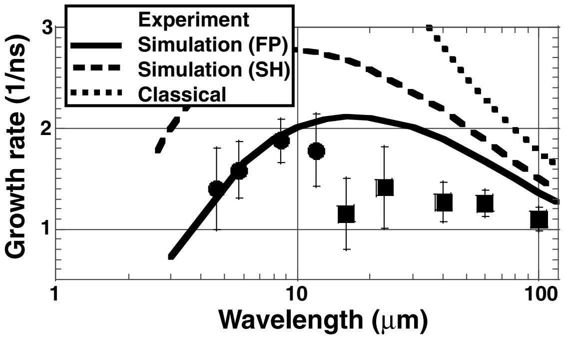

FIG. 4. The dispersion curve of the RT growth rate and the experimental data. Fokker-Planck simulation (solid curve) indicates closer agreements with the experimental results (closed circles and squares) rather than Spitzer-Härm simulation (dashed curve).

thus increasing the ablation velocity [9,10] and the density scale length [11]. Indeed, in the present experimental conditions, the ratio of electron mean-free-path and the temperature scale length is calculated to be $\sim 1/10$ from the ILESTA-1D. The experimental results are in considerably better agreement with the simulation results of the Fokker-Planck equation for nonlocal heat transport than that of the Spitzer-Härm case. The densities of the ablation front were nearly constant while the target is accelerating and were calculated to be about 2.1 $\mathrm{g/cm^3}$ for the Spitzer-Härm case and about 1.6 $\mathrm{g/cm^3}$ for the Fokker-Planck case. The density scale length ($L = 1.5\ \mu\mathrm{m}$ at $t = 1.3$ ns) of the ablation front for the Fokker-Planck case was about 1.5 times as large as that of the Spitzer-Härm case. This indicates that the growth rate is reduced by the effect of both the density of the ablation front and the density scale length.

Although the Fokker-Planck simulation well reproduces the experiment at short wavelengths, there still exists a discrepancy between the simulation and the previous experiment at especially medium wavelengths ($\lambda \cong 20$–$60\ \mu\mathrm{m}$). One mechanism to account for the reduction is the modification of the ablative flow (enhanced dynamic overpressure). The ablative flow concentrates in the concave region of the target and thus blows the laser-absorption region far away from the target compared to that in the unperturbed case. Thus, at the concave region, the energy flux is reduced due to the increased distance between the ablation and the absorption region, thereby reducing the ablation pressure. The opposite is true for the convex region. This effect tends to reduce the perturbation amplitude. At short wavelengths, however, the perturbation of the ablative flow is fast reduced and thus the absorption region is unaffected. Previous theories include the dynamic overpressure, but do not include its enhancement due to the change of the laser absorption region.

In summary, the growth of the Rayleigh-Taylor instability at short wavelengths was measured for the first time with moiré interferometry. The Fokker-Planck simulation with Eq. (1) with $\beta = 1.7$ reasonably well reproduces the experimental results at short wavelengths. The growth rates are most likely explained by nonlocal heat transport, in which high-energy electrons in a tail of the Maxwell distribution penetrate into and preheat the target, thereby reducing the target density and thus increasing the ablation velocity and the density scale length.

We would like to acknowledge the dedicated technical support by the staff at the GEKKO XII facility for the laser operation, the target fabrication, and the plasma diagnostics

[1] S. Chandrasekhar, *Hydrodynamic and Hydromagnetic Stability* (Oxford University Press, London, 1968), Chap. 10.

[2] K. Nomoto *et al.,* Astrophys. J. **286**, 644 (1984); E. Livne and D. Arnett, Astrophys. J. **415**, L107 (1993).

[3] J. H. Oort and L. Spitzer, Jr., Astrophys. J. **121**, 6 (1955).

[4] S. Bodner, Phys. Rev. Lett. **33**, 761 (1974).

[5] H. Takabe *et al.,* Phys. Fluids **28**, 3676 (1985).

[6] R. Betti *et al.,* Phys. Plasmas **5**, 1446 (1998).

[7] H. J. Kull and S. I. Anisimov, Phys. Fluids **29**, 2067 (1986); J. Sanz, Phys. Rev. Lett. **73**, 2700 (1994); V. N. Goncharov *et al.,* Phys. Plasmas **3**, 1402 (1996); A. R. Piriz, Phys. Plasmas **8**, 997 (2001).

[8] M. Desselberger *et al.,* Phys. Rev. Lett. **65**, 2997 (1990); B. A. Remington *et al.,* Phys. Rev. Lett. **67**, 3259 (1991); C. J. Pawley *et al.,* Phys. Plasmas **6**, 565 (1999); J. P. Knauer *et al.,* Phys. Plasmas **7**, 338 (2000).

[9] H. Azechi *et al.,* Phys. Plasmas **4**, 4079 (1997).

[10] K. Shigemori *et al.,* Phys. Rev. Lett. **78**, 250 (1997).

[11] S. G. Glendinning *et al.,* Phys. Rev. Lett. **78**, 3318 (1997).

[12] K. S. Budil *et al.,* Phys. Plasmas **8**, 2344 (2001).

[13] M. Matsuoka *et al.,* Rev. Sci. Instrum. **70**, 637 (1999).

[14] M. Matsuoka, master's thesis, Osaka University, Osaka, Japan, 2000.

[15] H. Nakano *et al.,* Appl. Phys. Lett. **63**, 580 (1993); K. Mima *et al.,* Phys. Plasmas **3**, 2077 (1996).

[16] C. Yamanaka *et al.,* Nucl. Fusion **27**, 19 (1987).

[17] T. Endo *et al.,* Phys. Rev. Lett. **74**, 3608 (1995); T. Endo *et al., ibid.* **75**, 2908 (1995).

[18] R. D. Richtmyer, Commun. Pure Appl. Math. **13**, 297 (1960); E. E. Meshkov, Fluid Dyn. **4**, 101 (1969).

[19] N. Matsui *et al.,* J. Plasma Phys. **61**, 43 (1999).

[20] V. N. Goncharov, Phys. Rev. Lett. **82**, 2091 (1999).

[21] H. Takabe *et al.,* Phys. Fluids **31**, 2884 (1988).

[22] L. Spitzer and R. Härm, Phys. Rev. **89**, 977 (1953).

[23] A. R. Bell *et al.,* Phys. Rev. Lett. **46**, 243 (1981).

[24] A. Sunahara, *Annual Report of Institute of Laser Engineering* (Osaka University, Osaka, Japan, 1999), p. 295.

[25] T. D. Goldsack *et al.,* Phys. Fluids **25**, 1634 (1982).